Azimuthal asymmetry in elastic electron scattering by polarized $3P$ sodium atoms

Z. Shi,[1] C. H. Ying,[2] and L. Vušković[2]
[1]*Physics Department, New York University, New York, New York 10003*
[2]*Physics Department, Old Dominion University, Norfolk, Virginia 23529*
(Received 18 December 1995)

Azimuthal asymmetry of the differential cross sections between two polarized states has been measured in elastic electron scattering by laser-excited sodium atoms prepared in the $3\,^2P_{3/2}, F=3$ ($M_F=+3$ or $M_F=-3$) polarized state. These results are an observation of the orbital effect in the elastic electron collision due to M_L atomic state perpendicular to the scattering plane. Data are reported for electron energies in the range of 1–10 eV, comparable with the kinetic energy of the atomic valence electron. At polar scattering angle $\theta=135°$ we found the asymmetry to be more significant when the incident electron energy is lower. Differential cross sections of these excited, polarized states were obtained at 135° as a function of electron energy as well. The experimental results are compared with R-matrix-based close coupling, and convergent-close-coupling calculations. [S1050-2947(96)10206-7]

PACS number(s): 34.80.Bm

I. INTRODUCTION

Polarization-sensitive scattering studies have undergone significant development in nuclear [1] and atomic [2] physics because they reveal detailed aspects of a scattering process. Alkali-metal atoms have been more frequently chosen as targets for detailed study because of their theoretical simplicity and relative ease of experimental handling. Sodium, in particular, has been one of the most popular targets for electron scattering over the years. This is due in part to its relative ease in preparation, and in part to the coincidence that the sodium D_2 lines are at a wavelength appropriate for rhodamine dye, which is used effectively in dye lasers.

With the advent of tunable narrow-band lasers, especially cw dye lasers, it has become possible to study collisions with laser-excited atoms in their specific short-lived states. By use of the unique properties of the pumping laser light, namely, its monochromaticity, well-defined polarization, and high intensity, one can achieve the excited-state population of the target atom in the scattering region to be comparable to the ground-state population and study in detail fine-structure or even hyperfine-structure transitions, or transitions between different magnetic substates.

A considerable number of experiments were performed on sodium using polarized electron beams by groups at National Institute for Standards and Technology (NIST) and University of Münster. Researchers at NIST have performed a series of elastic and superelastic scattering measurements. They obtained spin asymmetries for superelastic scattering [3,4] from the $3\,^2P_{3/2}$ excited sodium, the spin asymmetry for ground-state elastic scattering [5,6] from spin-polarized sodium atoms, and the ratio [7] of triplet to singlet elastic scattering cross sections. Researchers at University of Münster measured [8] left-right asymmetries for spin-polarized electrons scattered superelastically from laser-excited unpolarized sodium atoms.

We performed an experimental investigation on elastic electron scattering (unpolarized electrons are used here) with laser-excited polarized sodium atoms [9]. The aim of this research is to study the azimuthal asymmetry caused by a so-called ''orbital effect'' in the collision when the target atom is oriented with an orbital angular momentum perpendicular to the scattering plane. The laser-excited, polarized $3P$ sodium atom is an ideal target to study this orbital effect, since almost 100% atomic polarization can be achieved by excitation with polarized laser light, and its relatively small spin-orbit interaction can be neglected [5] in this process. Such an orbital effect is a consequence of the pure Coulomb interaction between the valence and the projectile electrons.

A simple classical picture to explain this orbital effect is given in Fig. 1. The polar scattering angle θ lies in the scattering plane defined by the collision frame [2] [electron (z) and atom ($-x$) axes of propagation, $\theta=0°$ along $+z$ axes], and the projection of the azimuthal scattering angle ϕ lies in the plane of atom and photon ($-y$) propagation axes. In such a configuration collisions in the scattering plane correspond to ($\theta, \phi=0°$) and ($\theta, \phi=180°$). By employing a circularly polarized laser light propagating perpendicularly to

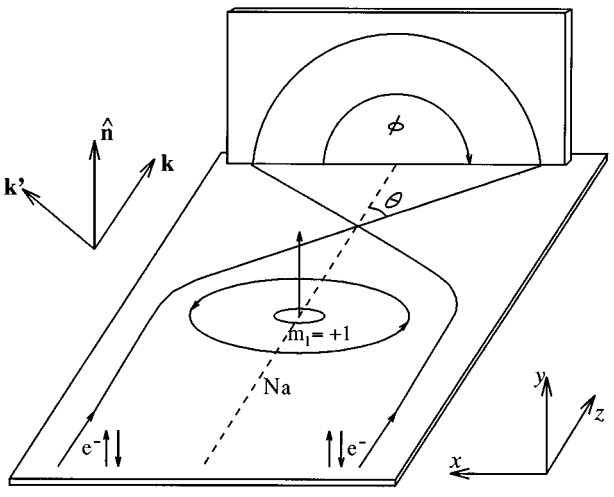

FIG. 1. Classical picture of orbital effect. Propagation of photon, atom, and electron beams are along $-y$, x, and z axes, respectively. The wave vectors of the continuum electron before ($\mathbf{k}$) and after ($\mathbf{k}'$) collision define the scattering plane $\hat{\mathbf{n}}$.

the scattering plane, a sodium atom can be excited and polarized in one of its pure $3P$ states, e.g., $3\,^2P_{3/2}, F=3, M_F=3$, in which the orbital angular momentum is also in a pure magnetic substate $M_L=+1$ and the quantum axis is perpendicular to the scattering plane. Under such a condition, when the projectile electron passes the target sodium atom from the left (or right) and scattered into a polar angle θ and an azimuthal angle $\phi=0°$ (or 180°), the valence electron and the projectile electron will move ''parallel'' (or ''antiparallel'') to each other during the collision. In that case, the effective interaction due to the Coulomb repulsive force between the two electrons during the collision process that determines the momentum transfer is different. Thus, in such a collision process an azimuthal asymmetry [Eq. (17) in Sec. III] in the differential cross-section measurements is expected. This asymmetry [9] is expected to be more significant at low incident energies and large scattering angles. It is worth noting that from reflection symmetry consideration the azimuthal asymmetry is equivalent to the asymmetry in differential cross-section measurements at a fixed azimuthal angle between initially opposite polarized target states. Since an unpolarized electron beam was employed in the present experiment the spin-orbit asymmetry [7] is excluded.

In this paper we present the azimuthal asymmetry of the differential cross sections in elastic electron scattering by polarized $3P$ sodium atoms obtained experimentally. The relative differential cross sections (DCS) of the elastically scattered electrons at $(\theta=135°, \phi=0°)$ and $(\theta=135°, \phi=180°)$ for both ground and $3^3P_{3/2}, F=3$ ($M_F=+3$ or $M_F=-3$) states of sodium were also obtained for the incident electron energy range from 1 to 10 eV. An absolute DCS for $3P$, $M_L=\pm 1$ at $\theta=135°$ as a function of electron energy was determined when the ground-state DCS's were put on the absolute scale with respect to theory.

An overview of the experimental method employed in the present research as well as the measured quantities are presented in Sec. II. The relationship between experimentally obtained data and the calculations is discussed in Sec. III, while the final results of azimuthal asymmetry and absolute DCS's for $3P, M_L=\pm 1$ states are presented in Sec. IV.

II. EXPERIMENT

A crossed-beam apparatus was used to perform the experiment. It was constructed [10–12] to be suitable for electron scattering by atoms using the atomic-recoil technique. Without changing the original options to observe atoms recoiled by the electron, the photon, or both, we reconstructed [13] an interaction system in order to observe the scattered electrons as well. In this interaction system a collimated electron beam with low energy (1–30 eV) can be produced by an electron gun and cross fired with an atom beam. The electrons scattered to the polar angle $\theta=135°$ with azimuthal angles $\phi=0°$ and $\phi=180°$ can by energy analyzed and detected. For convenience we recall briefly the essential parts of the apparatus. Additional experimental information and the interaction system are presented.

As explained in the previous section, the propagation axes of the atom beam, incident electron beam, and laser beam are mutually perpendicular to each other. The scattering plane is

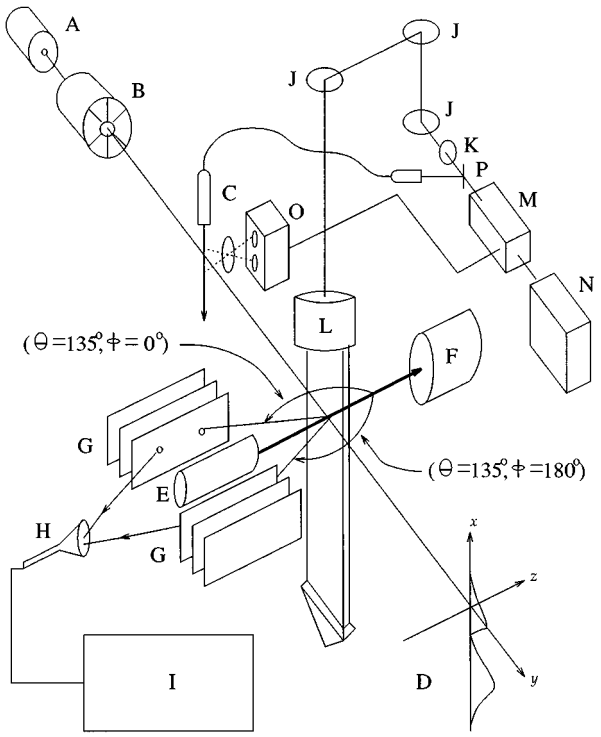

FIG. 2. Schematic diagram of experimental setup: *A*, sodium source; *B*, 6-pole magnet; *C*, fiber; *D*, detector plane; *E*, electron gun; *F*, Faraday cup; *G*, electron energy analyzers; *H*, channeltron; *I*, counting system; *J*, steering mirrors; *K*, circular polarizer; *L*, cylindrical lens telescope; *M*, dye laser; *N*, Ar^+ laser; *O*, laser stabilization system; *P*, beam spitter.

defined by the initial ($\mathbf{k}$) and scattered electron ($\mathbf{k}'$) momentum vectors (see Fig. 1). Electrons scattered into the polar angle $\theta=135°$ with azimuthal angles $\phi=0°$ and $\phi=180°$ were detected.

The apparatus consists of four stainless-steel vacuum chambers: the source chamber containing an atom beam source and a skimmer, the baffle chamber containing a laser stabilization system, the interaction chamber containing the interaction system, and the atom beam detection chamber containing a hot wire atom detector. There is a hexapole magnet between the source and the baffle chambers that can focus and partially velocity and state select the atom beam. The overall length of the apparatus is close to 5 m. One unique part of the apparatus is the atom beam detection chamber, which is connected to the interaction chamber through a 3.35-m-long drift tube by attaching to a rotary altazimuthal mount. The atom beam profile as well as the recoiled atoms due to electron collision or photon absorption spatial distribution can thereby be scanned two dimensionally on the surface of a sphere centered at the interaction region. The sodium atom beam was produced by the high-temperature oven. The pressure in the system during the operation at 830-K oven temperature was 1×10^{-6} torr in the source chamber, 1×10^{-7} torr in the baffle chamber, and $(1–4)\times10^{-8}$ torr in the collision and in the atom beam detection chambers.

A schematic diagram of the experimental setup is shown in Fig. 2. Excited $(3P)$Na atoms were prepared by a cw

single-mode ring dye laser (Coherent-699-21 with Rhodamine 6G) tuned to the $3\,^2S_{1/2}, F=2 \rightarrow 3\,^2P_{3/2}, F=3$ transition and polarized in one of the magnetic substates ($M_F=+3$ or $M_F=-3$) by employing σ^+ or σ^- circularly polarized laser light propagating perpendicularly to the scattering plane [14,15]. The orbital angular momentum (see Fig. 1) was also in a pure magnetic substate $M_L=+1$ or $M_L=-1$, quantized along the laser propagation axis (natural frame [2]). The dye laser is pumped by a 6-W, 514.5-nm, TEM_{00} mode argon-ion laser (Coherent CR-15 SG). Under optimum conditions the output power of the ring dye laser can be 1.2 W for broadband radiation and 600 mW for single-mode radiation around the sodium D_2 line of 589.0 nm. The effective linewidth of the single-mode output was about 1 MHz. In the lock mode, even with a temperature stabilized reference cavity, there was still a frequency drift about 100 MHz/h. In order to achieve a better performance of the laser, a frequency stabilization feedback system has been developed and implemented [13]. This system, fully described in a forthcoming publication [16], is based on a Doppler shift due to radial velocity spread of the atomic beam itself. So the laser frequency was kept within 1 MHz over 20 h. During the experiment a Fabry-Pérot interferometer (Spectra-Physics 470) with a 2-GHz free spectral range was used to monitor the mode structure of the laser beam and to display on an oscilloscope. A sodium vapor cell heated up to 80 °C was used for coarse tuning of the sodium D_2 line transition. An optical fiber was used to transfer a probe laser beam (about 1 mW) for atom beam diagnosis and frequency fine tuning. A broadband polarization rotator (Spectra Physics 310-21) and a quartz zero-order quarter-wave plate were placed in the path of the laser beam to achieve circular polarizations of the light. The main beam was reflected by three mirrors onto the scattering apparatus, shaped by a cylindrical lens telescope into a ribbon-shaped beam, about 5 cm long and 0.5 cm wide to illuminate the atom beam in the interaction region at right angles.

A special electron gun was designed and built to fulfill the requirements of this experiment, which include good collimation, high beam intensity, and low electron energy with narrow energy spreading. The design of the electron gun [13] was based on computer simulation results using the SIMION program [17]. The electron emitting source is a tungsten dispenser cathode (Spectra-Mat, Inc. No. 134), which has an emitting area of 9.1 mm^2 and an emitter thickness of 1.0 mm. The cathode body, 7.2 mm in length is made of molybdenum. There are three brazed legs attached to the body providing good thermal isolation and mounting flexibility. One leg was also used as an electrode with a base voltage that determines the electron energy. The operating temperature of the cathode was between 800 °C and 1025 °C. The dc current of the resistive heater is in the range of 1.2–1.7 A for a stable performance. At these temperatures the saturated dc emissions were 3–9 A cm^{-2}, which were much more than the present requirements. It was not necessary to keep the temperature of the cathode very high to achieve large electron currents, which was limited by the space charge. The electrodes (slits, grid, spacers) of the electron gun were built from molybdenum. Electrical insulators between the electrodes were laser machined 0.37-mm-thick ceramic chips (Sheffield Precision Ceramics Company). The envelope of the electron gum made of titanium was grounded electronically to shield the interaction region from the electrical fields produced by the electrodes. The whole electron gun together with the collector and energy analyzers (explained later in this section) was mounted on a stainless-steel holder, which was connected through a flexible bellows to a positioner outside the vacuum chamber. The positioner can be movable in three dimensions and rotatable along the electron beam axis.

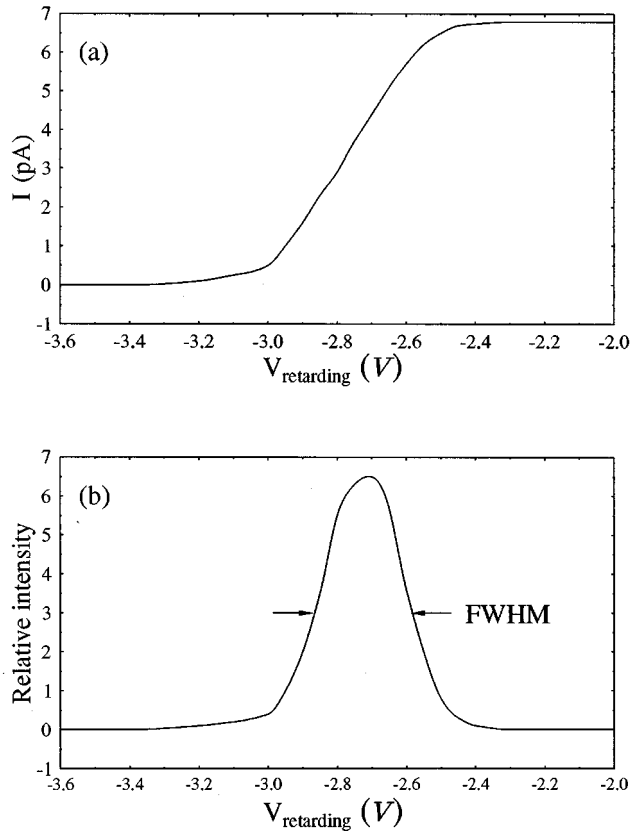

FIG. 3. Incident electron energy distribution: (a) measured electron current as a function of the retarding potential; (b) energy distribution obtained by differentiating curve (a).

A primary electron beam collector was installed in order to diagnose the electron beam. It consists of two Faraday cups and one retarding plate between them. Results of the electron beam energy distribution shown in Fig. 3 were measured employing the retarding potential method. The full width at half maximum (FWHM) was found to be about 0.3 eV and it was almost unchanged when the energy of the electrons was changed from 1 to 10 eV. One can conclude that this energy distribution was mainly due to the thermal energy spreading of the heated cathode. The primary electron beam currents were in the range of 10^{-7}–10^{-5} A depending on the electron energy. They were limited only by the space charge effect, which can be expressed [18] by

$$I_{\max}\ (\mu\mathrm{A}) = 38.5[E_0^{3/2}(\mathrm{eV})]a^2/b^2, \tag{1}$$

where $I_{\max}$ is the maximum achievable current, E_0 is the electron energy, a is the diameter of the electron beam cross section (same as the exit aperture of the electron gun), and b is the collimation length. In the present case where $a=1$

TABLE I. The measured maximum incident electron current at a given energy with corresponding voltages applied on the cathode, grid, and focusing electrode.

E_0 (eV)	V_{cathode} (V)	V_{grid} (V)	V_{focus} (V)	$I_{\max}$ (μA)
1.0	−3.4	−1.4	10	0.30
2.0	−4.4	−2.1	12	0.80
3.0	−5.4	−2.8	14	1.3
4.0	−6.4	−3.6	15	2.6
5.0	−7.4	−4.3	17	3.6
6.0	−8.4	−4.9	20	4.2
7.0	−9.4	−5.7	22	5.3
8.0	−10.4	−6.2	25	6.8
9.0	−11.4	−7.0	28	8.3
10.0	−12.4	−7.8	30	9.0

mm and $b \approx 10$ mm, for $E_0 = 1$ eV, $I_{\max} \approx 3 \times 10^{-7}$ A and for $E_0 = 10$ eV, $I_{\max} \approx 9 \times 10^{-6}$ A. These calculated results were very close to the measured maximum electron currents at a given energy, which are presented in Table I. The indicated electron beam currents where measured on the primary electron beam collector whose components were set to 60 V to achieve saturated collection. In the same table are listed voltages applied at each electrode of the electron gun during $I_{\max}$ measurements. These are the cathode bias voltage V_{cathode}, grid voltage V_{grid}, and focusing voltage V_{focus}. Basically, V_{cathode} determines the electron energy, V_{grid} accelerates the electrons from the cathode and mainly controls the intensity of the electron beam, and V_{focus} determines the collimation of the beam and slightly affects the intensity. The electron beam energies E_0 listed in column 1 are nominal (corrected) energies. This energy can be expressed as

$$E_0 = -e(V_{\text{cathode}} - V_{\text{correction}}), \tag{2}$$

where $V_{\text{correction}}$ includes the contact potential correction and space charge correction. The relative contact potential voltage difference can be obtained when the retarding potential method was used by determining the energy distribution. It is found to be about 1.7 V. The space charge correction can be estimated when the intensity and dimensions of the electron beam are known. In Fig. 4 we plotted the data of $I_{\max}$ versus V_{cathode}. According to Eqs. (1) and (2) and assuming that $V_{\text{correction}}$ is a constant in the zeroth-order approximation, one can adjust and determine the value of $V_{\text{correction}}$ as a parameter by fitting the curve $I_{\max} \propto E_0^{3/2} \propto (V_{\text{cathode}} - V_{\text{correction}})^{3/2}$. Using this method, we found that the best fitting corresponds to the proportionality constant of 0.3 and $V_{\text{correction}} = 2.4$ V as shown in Fig. 4. Another method to perform electron beam diagnoses of FWHM and E_0 will be explained later in this section.

In order to reduce the magnetic field in the interaction region a cylindrical double-walled high permeability μ-metal shielding was used around the whole interaction system in the vacuum chamber. The magnetic field inside the shielding was measured to be less than 20 mG. It was weak enough that one can neglect the magnetic field effects on the electron propagation, since the gyration radius of 1 eV electron in such magnetic field is larger than 1 m and the size of the whole interaction system with electron optics is only about 5 cm.

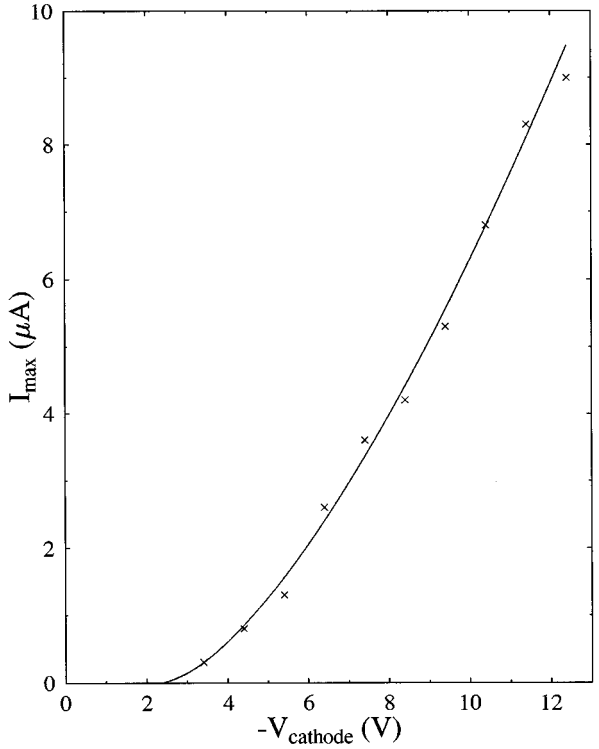

FIG. 4. Incident electron energy calibration: ×, maximized electron current at a given cathode voltage; full line, curve fitted by $I_{\max}(\mu\text{A}) = 0.3\{-[V_{\text{cathode}}(V)] - 2.4\}^{3/2}$.

The detection system used to measure the scattered electrons consists of two electron energy analyzers and a high gain (10^8) electron channeltron multiplier (Galileo Electron-Optics Corporation, Cat. No. 4860). The electron energy and analyzers (see Fig. 2) are two identical plane mirror analyzers where the scattered electrons are deflected and energy selected in a uniform static electrical field produced by two parallel electrode plates with the voltage difference V. In order to achieve a uniform electrical field inside of the analyzer and to reduce the edge effects, a third electrode plate at the potential of $V/2$ was placed at the middle of the two electrode plates. The middle plate has a slot in the center to let the electrons pass freely. During the experiment the inner electrode plate with the apertures was grounded, while the voltages on the middle and outer plates can be finely adjusted. The selected scattered electron energy E has a linear relationship with V as

$$E = \frac{eD}{2r \sin 2\alpha} V, \tag{3}$$

where e is the electron charge, D is the electron traveling focal length, which is equivalent to the distance between the centers of the entrance and exit apertures of the analyzer, r is the separation between the two electrode plates, and α is the electron incident angle. The electrode plates of the analyzers were parallel to the electron primary beam and placed back on the two sides of the electron gun. Thus, to detect electrons

scattered at ($\theta=135°, \phi=0°$) and ($\theta=135°, \phi=180°$), the incident angle $\alpha=45°$ is the same for both analyzers. The first advantage of such an incident angle is that the E and V have a simple relationship:

$$E=\frac{eD}{2r}V. \tag{4}$$

The second characteristic of the plane mirror analyzer at this incident angle is

$$\left.\frac{dD}{d\alpha}\right|_{\alpha=45°}=0. \tag{5}$$

This characteristic means that the analyzer has the same focal length D for all electrons whose incident angles are near around $\alpha=45°$. Due to the size of the entrance and exit apertures, there is an uncertainty ΔD in the focal length that is mainly responsible for the energy resolution of the analyzer as

$$\Delta E/E \approx \Delta D/D, \tag{6}$$

where ΔE is the electron energy uncertainty, and

$$\Delta D=\sqrt{\Delta S_1^2+\Delta S_2^2}, \tag{7}$$

where ΔS_1 and ΔS_2 are the diameters of the entrance and exit aperature. In the present design the dimensions of an analyzer are (35.6 mm)×(20.0 mm)×(12.0 mm), while $D=15.2$ mm, $d=7.6$ mm, and $\Delta S_1=\Delta S_2=1.0$ mm. The electrode plates are made of molybdenum, while the spacers and the holders are of stainless steel. The electrical insulators are 0.37-mm-thick ceramic chips. Employing Eq. (6) the analyzer energy resolution is estimated to be $\Delta E/E \approx 10\%$. Its angular resolution is about $\pm 2°$, which is determined by the scattering volume and the sizes of the analyzer apertures as well as the distance between them. This angular resolution combined with the electron beam collimation of $\pm 2°$ defined the total angular uncertainty of $\Delta\theta=\pm 3°$.

Another way to find the exact electron energy E_0 and FWHM of the energy distribution is to analyze the elastic scattering peak in the background electron scattering spectrum taken by the energy analyzers. A typical spectrum with an elastic scattering peak and an inelastic scattering shoulder is shown in Fig. 5. The elastic scattering peak is due to both electron scattering by the residual gases in the interaction region and the surface scatterings, while the inelastic scattering shoulder is mainly due to the surface scattering. Data presented in Figs. 5(a) and 5(b) were taken at a pressure of 2×10^{-8} and 1×10^{-7} torr, respectively. The height of the elastic scattering peak is linearly proportional to the density of the residual gases, while the inelastic scattering shoulder is almost unchanged in different vacuum conditions. The linear proportionality between the elastic scattering peak and the density of residual gases is checked in the wide pressure range. The results obtained with 6-eV electrons are listed in Table II. The total counting time at each condition was 100 s. It was found that there is about a 10-Hz count from surface elastic scattering and about a 5-Hz count per 1×10^{-8} torr from the residual gases scattering. The shape of the electron background scattering spectrum taken with different electron

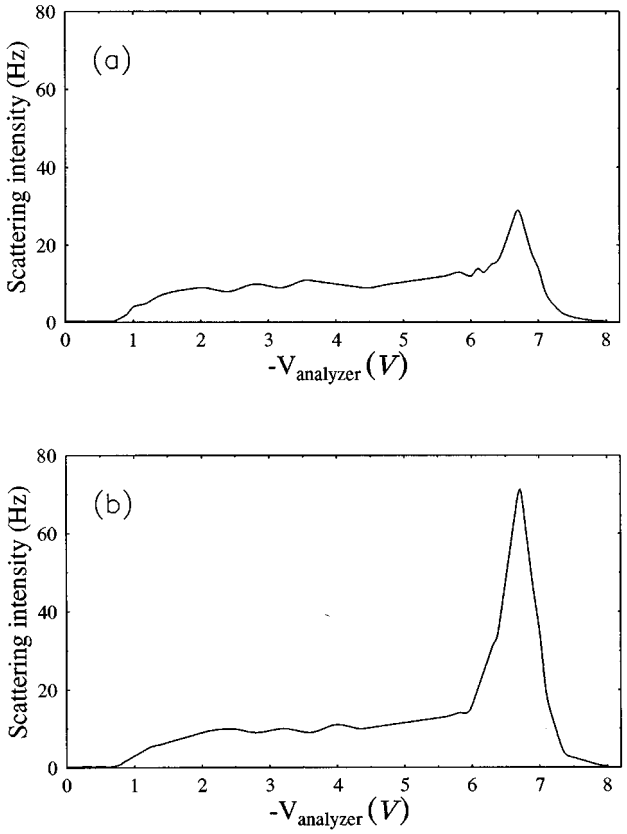

FIG. 5. Background electron scattering spectra taken with 6-eV incident electrons. The pressure in the interaction chamber: (a) 2×10^{-8} torr; (b) 1×10^{-7} torr.

energies was quite similar to that presented in Fig. 5. The actual electron energy in the scattering volume can be determined precisely from the elastic scattering peak. A contact potential correction for the energy analyzer electrodes of about 0.7 eV can be obtained from two facts. One, the inelastic scatterings shoulders always have a sharp cutoff voltage of about 0.7 V for all electron energies, and second, the lowest measurable elastic scattering peak was around 0.7 V. The electron energy determined by this method was quite consistent with the maximum current fitting method described above and presented in Fig. 4. The width of the elastic scattering peak was determined by both the primary electron beam energy distribution and the analyzer energy

TABLE II. The noise at the peak of elastic scattering at a given background pressure measured within counting period of 100 s.

Pressure (torr)	Counting rate (Hz)
1×10^{-8}	15
2×10^{-8}	19
4×10^{-8}	30
6×10^{-8}	42
8×10^{-8}	50
1×10^{-7}	61
2×10^{-7}	112
3×10^{-7}	158
4×10^{-7}	206

TABLE III. Full width at the half maximum (FWHM) of the elastic scattering peak obtained from the background scattering spectrum.

E_0 (eV)	FWHM (eV)
1.0	0.32
2.0	0.35
3.0	0.42
4.0	0.50
5.0	0.59
6.0	0.70
7.0	0.75
8.0	0.88
9.0	1.0
10.0	1.1

resolution. From the measured FWHM of the elastic scattering peak at different incident electron energies presented in Table III, it was confirmed that the primary electron beam had a distribution of 0.3 eV at FWHM and the energy resolution of the analyzer was about 10% of the electron energies. All the diagnosis procedures were done before the scattering experiment was performed. During the scattering experiment an additional primary electron beam collector as a damping absorber was used to achieve maximum absorption of the primary electrons so that the background scattering signals from the surrounding surface can be minimized.

When the sodium atom beam was present the elastic electron scattering signal was about 2–4 Hz. The corresponding estimated sodium atom density was about 2×10^{8} cm^{-3}. The experiment was performed with this relatively low atomic beam density because its good collimation was crucial since the population of excited state sodium atoms have to be determined from the atom beam profile measurement. Since the background noise was almost a constant, by chopping the atom beam the noise can be reduced to the limit of the counting fluctuations. Thus, by increasing the data taking time as long as the experimental conditions were stable, the statistical error can be reduced to a level comparable to other uncertainties in the experiment.

For initial atom state preparation a traveling-wave laser field [19] was arranged in which the laser light passes through the interaction region in one direction. The excited-state relative population was determined by measuring the deflected atomic beam profile due to resonant photon absorption (see Fig. 6). The fraction f of the excited-state atoms in the interaction region is equivalent to the fraction of time an atom spends in the excited state while it is exposed to the laser field. For convenience, we recall its relation [13,19] to the deflection displacement d of the atom beam profile

$$f=\frac{MV^2\lambda\tau_0 d}{hLl}, \tag{8}$$

where M is the mass of sodium atom, $V=1200$ m/s is the mean velocity of the atom beam, $\lambda=5890$ Å is photon wavelength, $\tau_0=1.6\times10^{-8}$ s is the lifetime of the $3P$ excited state, h is the Planck constant, $L=3.35$ m is the distance between interaction region and the atom beam detector plane, and $l=15.2$ mm is the laser radiation length, respectively. From deflection measurements $d=17$ mm was obtained. Thus, the fraction of the excited states was about 25% according to Eq. (8). The calculated value of f is actually an average result. First, the atom beam possesses a velocity distribution $\mathbf{V}(V)$. Second, since the center of the scattering volume is in the middle of l, in a first-order approximation f in the scattering volume is taken to be the same as the average f along the interaction path l. Of course, the lifetime τ_0 has only its statistical meaning and the spontaneous emission will result in a random walk broadening of the atom beam profile. After considering all these effects as well as the uncertainties in the measurements, a 10% error in f determination was estimated. The measured relative excited-state population f was found to be the same for both polarized states. Detailed discussion about power broadening, optical pumping, and frequency detuning effects can be found in our previous work [20–23].

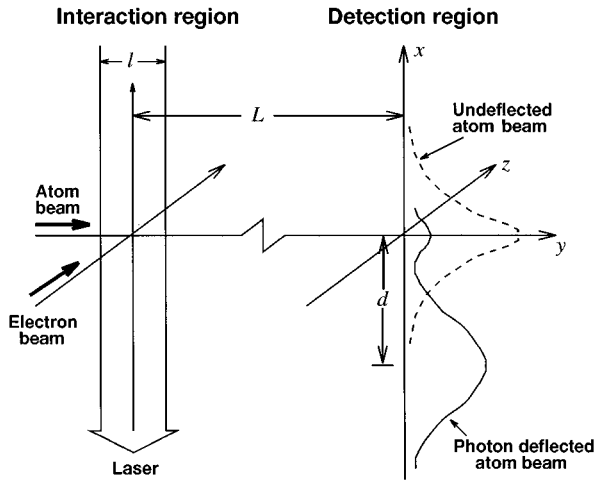

FIG. 6. Scheme of traveling-wave arrangement for measurements of the fraction of the excited-state atoms, f: l, the laser radiation length; L, the distance between interaction region and the atom beam detector plane; d, the atomic beam deflection.

The primary electron beam intensity and the atom beam flux are always monitored during the data taking period. The fluctuations were kept below 1% and 3%, respectively. By chopping the sodium atom beam, the electron scattering signal from the ground-state sodium atom was measured using each analyzer alternatively. Thus, the relative efficiency of the two analyzers was determined. The chopping frequency has been changed from 1 to 0.01 Hz to check the consistency of the signal at different chopping frequencies. By chopping the laser light as well as the atom beam (see Fig. 7), electron scattering signals from excited-state sodium atoms at both azimuthal angles were measured. The ground-state scattering signal (N) taken with laser-off and scattering signal from the mixture of ground- and excited-state atoms ($N^{\pm}$) taken with laser on were measured, where the $\pm$ sign refers to $M_L=\pm1$. The measurement was repeated at each energy on different days at least three times. The final results are presented as an average of all the measurements for each electron incident energy. For convenience, the typical experimental parameters are summarized in Table IV.

In this experiment only relative measurements were required. Thus, all the parameters, such as atom density, elec-

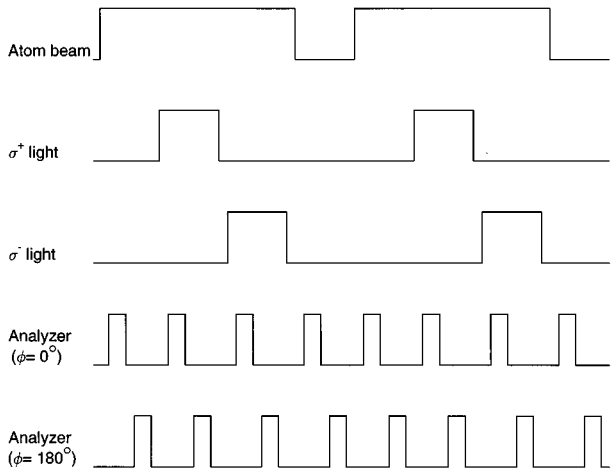

FIG. 7. Data taking scheme with indicated relative chopping duration.

tron current, scattering volume, solid angle, and detection efficiency can be expressed by only one coefficient η to link the signal counting rate to the differential cross section σ. The scattering intensities N and $N^{\pm}$ can be expressed as

$$N=\eta\sigma_{3S}, \tag{9}$$

$$N^{\pm}=\eta[(1-f)\sigma_{3S}+f\sigma_{3P}^{\pm}], \tag{10}$$

where σ_{3S} is the sodium $3S$ ground-state scattering cross section and $\sigma_{3P}^{\pm}$ is the sodium $3P$ excited-state scattering cross sections for different polarized states.

From reflection symmetry considerations, the scattering intensity at $(\theta,\phi=0°)$ for $M_L=+1$ is equal to the intensity at $(\theta,\phi=180°)$ for $M_L=-1$. One can experimentally double check this asymmetry by comparing signals at $(\theta,\phi=0°)$ and $(\theta,\phi=180°)$ for a chosen M_L state, and by comparing signals for $M_L=+1$ and $M_L=-1$ states at a chosen angle (θ,ϕ). Both types of observation were employed in the present experiment with consistent results obtained. The final asymmetry results are the average value of data taken at the two azimuthal angles. In these measurements the polarization of laser light was changed at the fixed azimuthal angle. An advantage of this approach is that calibration of η between the two analyzers is not needed. The measurements taken with fixed laser light at different azimuthal angles were only used as a test of consistency. With this experimental approach, calibration of η would be required to obtain the final results, which would introduce an additional uncertainty.

TABLE IV. Experimental parameters.

Parameters	Values
Electron current	0.3–9 μA
Electron beam diameter	0.10 cm
Oven source temperature	830 K
Nozzle temperature	900 K
Sodium beam average velocity $\overline{V}$	1200 m/s
Nozzle orifice diameter	0.040 cm
Sodium beam diameter	0.15 cm
Sodium density N_{atom}	2×10^{8} cm^{-3}
Vacuum in interaction chamber	2×10^{-8} torr
Residue magnetic field	<20 mG
Laser power intensity	100 mW/cm^2
Degree of circular polarization p	$>97\%$
Laser interaction length l	1.52 cm
Photon recoil atom deflection d	1.7 cm
Related excited state population f	25%
Angular uncertainty $\Delta\theta$	$\pm3°$
Scattering volume	1 mm^3
Background noise	20–100 Hz
Ground state scattering signal N	2–4 Hz
Scattering signal with laser on $N^{\pm}$	2–5 Hz

TABLE V. Uncertainties of measured quantities.

Measured quantities	Uncertainties
Atom beam fluctuation	3%
Vacuum pressure	$<1\%$
Electron current measurement	$<1\%$
Degree of atomic polarization p	3%
Atom scattering signal	5%
Determination of f	10%
$\sigma_{3P}^{\pm}$ measurements	20%–30%
Azimuthal asymmetry A	±0.05–±0.15

The main uncertainties of the present experiment come from the counting statistical errors due to large background noise, the relative excited-state population f measurement, and the degree of atomic polarization p determination. These uncertainties, summarized in Table V, all are at the 1σ (68%) confidence level. The final counting uncertainty can reach the level of 0.1 Hz if the repeated measurements at different data taking sessions were averaged, and total data acquisition time for each signal was over 2500 s during one session. The atom scattering signal (2–4 Hz) was measured with only a 5% statistical uncertainty. It almost reaches the limitation of the atom beam fluctuation, which was 3%. The stability of the vacuum pressure in the interaction chamber and the steadiness of the electron current determined the reliability of the measurements done by the chopping method. Any visible long-term variations, longer than the chopping period, had to be corrected for. Since only one-fourth of the atoms are in their excited states, which contribute to the excited-state scattering signals, the statistical uncertainties in the $\sigma_{3P}^{\pm}$ determinations were enlarged almost four times (up to about 20%) comparing with σ_{3S} determinations. Considering the uncertainties in f determination (10%) and polarization degree p measurement (3%), the uncertainty of $\sigma_{3P}^{\pm}$ determination were even larger (20%–30%).

III. THEORETICAL DESCRIPTION

In order to fully understand the collisional dynamics, a number of methods have been developed to describe the electron-atom scattering process, which is basically a many-body problem. In the low incident electron energy range where the present experiment has been performed, the proper

theoretical calculation employs the close-coupling approximation. Motivated by this experiment, numerical data have been calculated employing a ten-state close-coupling (CC) approximation [24] based on an R-matrix method at incident electron energies up to 3 eV [25], and employing a convergent-close-coupling (CCC) approximation [26] in the energy range from 1–10 eV. All these calculations yield the scattering amplitudes or the reduced T-matrix elements and all the experimentally observable quantities can be related to them. For example, the measured scattering intensity for a specific transition $i \rightarrow j$ can be expressed as

$$I(\theta,\phi) = \eta \frac{d\sigma}{d\Omega}\bigg|_{j\leftarrow i} = \eta \frac{k_j}{k_i} |f_{ji}(\theta,\phi)|^2, \tag{11}$$

where η includes experimental parameters. $d\sigma/d\Omega|_{j\leftarrow i}$ is the differential cross section for the $i \rightarrow j$ channel. k_i and k_j are the scattered electron initial and final wave number. $f_{ji}(\theta,\phi)$ is the scattering amplitude. In general, the initial and final states are selected only with some probability. The measured intensity corresponds to

$$I(\theta,\phi) = \eta \frac{k_j}{k_i} N_j \mathrm{Tr}(\boldsymbol{\sigma}_{\mathrm{det}} \mathbf{F} \boldsymbol{\sigma}_{\mathrm{prep}} \mathbf{F}^{\dagger}), \tag{12}$$

where $\boldsymbol{\sigma}_{\mathrm{det}}$ is an $N_j \times N_j$ matrix describing the analysis of the final state, $\boldsymbol{\sigma}_{\mathrm{prep}}$ is an $N_i \times N_i$ matrix describing the preparation of the initial state, and $\mathbf{F}$ is an $N_j \times N_i$ scattering matrix whose elements $\langle j|\mathbf{F}|i\rangle = f_{ji}$ are the standard scattering amplitudes. N_i and N_j are the number of any possible initial and final states, respectively.

In the present experiment the initial atomic state was prepared by circularly polarized laser light and all possible final magnetic substates were detected with equal efficiencies, so

$$\boldsymbol{\sigma}_{\mathrm{det}} = N_j^{-1} \mathbf{1}, \tag{13}$$

where $\mathbf{1}$ is the unit matrix.

As mentioned in the previous section, by optical pumping with σ^+ light (or σ^- light), one can produce excited sodium in its pure $3\,^2P_{3/2}, F=3, M_F=3$ (or $M_F=-3$) state in the natural frame [2]. The atom is also in its initial pure $L=1, M_L=1$ (or $M_L=-1$) magnetic substate. The preparation density matrix in the natural frame has a simple form for σ^+ light,

$$\boldsymbol{\sigma}^{+}_{\mathrm{prep}} = \begin{pmatrix} 1 & 0 & 0 \\ 0 & 0 & 0 \\ 0 & 0 & 0 \end{pmatrix}, \tag{14}$$

and for σ^- light,

$$\boldsymbol{\sigma}^{-}_{\mathrm{prep}} = \begin{pmatrix} 0 & 0 & 0 \\ 0 & 0 & 0 \\ 0 & 0 & 1 \end{pmatrix}. \tag{15}$$

Usually the scattering amplitudes are calculated in the collision frame [2]. Transformation from the collision frame to natural frame can be performed [27] by standard rotation matrix $\mathbf{D}$ (α,β,γ) with the Euler angles being $-\pi/2, -\pi/2, 0$, respectively.

For unpolarized electrons the scattering is a mixture of singlet (s) and triplet (t) spin state, thus the spin-average differential cross section is

$$\sigma(\theta) = \tfrac{1}{4}\sigma(\theta)^s + \tfrac{3}{4}\sigma(\theta)^t. \tag{16}$$

Inserting σ_{prep} defined by Eqs. (14) and (15) into Eq. (12), one can obtain the elastic differential cross section $\sigma^{\pm}_{3P}$ for $M_L = \pm 1$ polarized states. Than, the azimuthal asymmetry A can be defined as

$$A = \frac{\sigma^{+}_{3P} - \sigma^{-}_{3P}}{\sigma^{+}_{3P} + \sigma^{-}_{3P}}. \tag{17}$$

From a theoretical point of view, this asymmetry can be simply related [26] to one of the reduced Stokes parameters as

$$A = -P_3. \tag{18}$$

The orientation parameter $L_\perp$ defined as the angular momentum transfer to an initially unpolarized atom target (or a final unpolarized atom for a proper time-reversal process) is often used to describe the collision process. This parameter can be also related to A [26] as

$$L_\perp = A(1-\rho^n_{00}), \tag{19}$$

where ρ^n_{00} is the natural frame density matrix element for the $M_L=0 \rightarrow M_L=0$ transition. Unlike in the $3^2P \leftrightarrow 3^2S$ transition where ρ^n_{00} vanishes due to the symmetry restriction, ρ^n_{00} is nonzero in the $3^2P \leftrightarrow 3^2P$ collision process. Thus, $L_\perp$ is no longer equal to $-P_3$. In order to determine $L_\perp$ experimentally one has to determine ρ^n_{00} independently. The experimental arrangement with circularly polarized laser light used in the present work to determine A can also be used to determine ρ^n_{00} if linearly polarized laser light is used to prepare the initial atomic state. In order to obtain ρ^n_{00} from such experiment, it would be necessary to normalize the scattering intensities that correspond to the initial atomic states prepared with differently polarized laser light.

IV. RESULTS AND DISCUSSION

We obtained scattering intensities N, N^+, and N^- at a fixed polar angle $\theta = 135°$ in order to examine the asymmetry due to orbital effect in the elastic differential cross sections between the two sodium polarized excited states $3P, M_L=+1$ and $3P, M_L=-1$. These scattering intensities, measured at incident energies 1–10 eV and presented in Table VI, are related to the relative DCS's of ground and excited states according to Eqs. (9) and (10). A fraction of excited sodium atoms f has been measured as well. Combining Eqs. (9), (10), and (17) one can derive azimuthal asymmetry with respect to measured quantities N, N^+, N^-, and f as

$$A = \frac{N^+ - N^-}{N^+ + N^- - 2(1-f)N}. \tag{20}$$

The asymmetry results obtained according to Eq. (20) are presented also in Table VI as a function of electron energy.

TABLE VI. Measured scattering intensities of the ground state (N) and mixture of ground and excited state with $\sigma^+(N^+)$ or σ^- (N^-) laser light, and obtained azimuthal asymmetry (A) and differential cross sections of $3P,M_L=+1$ (σ^+_{3P}) and $3P,M_L=-1$ (σ^-_{3P}) as a function of incident electron energy. Data are taken at polar scattering angle of 135 °. Cross sections are in the units of 10^{-20} m^2/sr.

E_0 (eV)	N (Hz)	N^+ (Hz)	N^- (Hz)	A	σ^+_{3P}	σ^-_{3P}
1.0	2.85	4.15	3.25	0.29	13.0	7.2
2.0	3.1	5.2	3.75	0.34	4.9	2.4
3.0	2.7	4.1	3.25	0.26	1.0	0.60
4.0	3.45	4.05	3.5	0.23	0.48	0.30
5.0	3.55	3.85	3.5	0.17	0.29	0.21
6.0	3.6	3.8	3.55	0.13	0.22	0.17
7.0	2.7	2.9	2.7	0.13	0.14	0.10
8.0	2.25	2.15	2.05	0.12	0.071	0.063
9.0	2.45	2.35	2.25	0.11	0.067	0.052
10.0	2.1	2.0	1.95	0.06	0.049	0.044

These data are plotted in Fig. 8 together with calculated results [25,26]. The indicated error bars correspond to 1σ (68%) confidence level. Calculated results are in good agreement with the experiment. However, the measured asymmetry is generally less significant. The CC calculated results show a pronounced structure in the energy region 1–2.5 eV where the thresholds for the $4S$, $3D$, and $5S$ channels are located. Due to limited energy resolution of the experiment, these structures cannot be tested. The CCC calculated results [26], presented with discrete points, show the maximum at

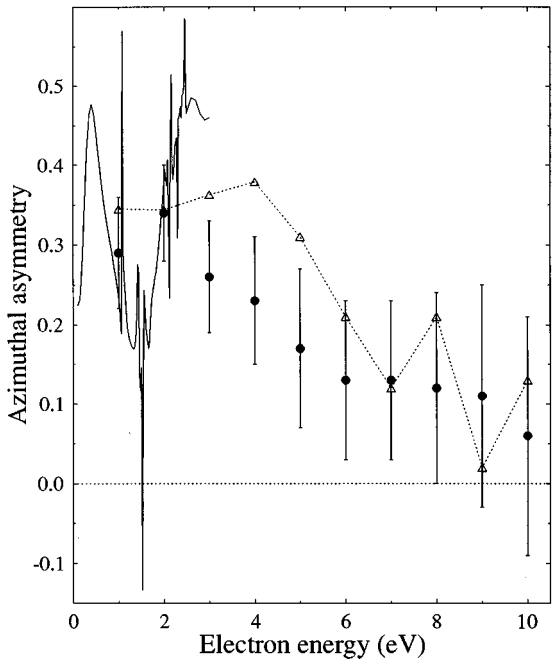

FIG. 8. Azimuthal asymmetry at polar scattering angle 135° for elastic scattering of unpolarized electrons by laser excited, polarized $3P,M_L=\pm1$ sodium states. Experiment: ●, present data with indicated error bars and the energy uncertainty of ±0.15 eV. Calculations: full line, close coupling [25]; △, connected with dashed line, convergent close coupling [26].

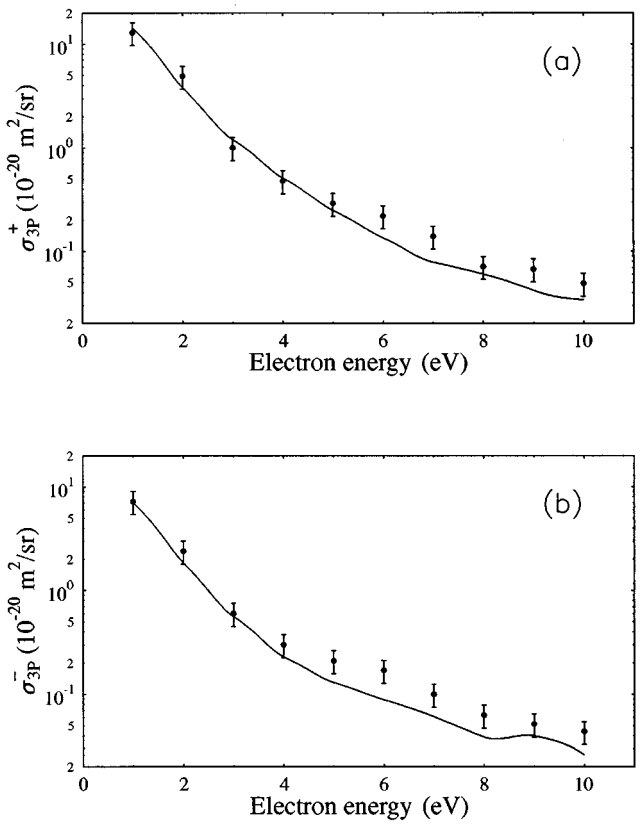

FIG. 9. Differential cross sections at polar scattering angle 135° for elastic scattering of unpolarized electrons by laser excited, polarized $3P,M_L=+1$ (a) and $3P,M_L=-1$ (b) sodium states. Experiment: ●, present data with indicated error bars and the energy uncertainty of ±0.15 eV. Calculation: full line, convergent close coupling [26].

higher energy than the experimental data. Also, an oscillation in calculated asymmetry around 8 eV has not been observed in the present data. Most likely, this oscillation is a shortcoming of the calculation due to difficulties with the convergence at the large scattering angles (see Fig. 6 in Ref. [26]).

Using the same measured quantities, the ratio of the elastic scattering DCS's between the $3P$ polarized states and $3S$ ground state can be obtained from Eqs. (9) and (10) as

$$\frac{\sigma^{\pm}_{3P}}{\sigma_{3S}}=\left(\frac{N^{\pm}}{N}-1\right)\Big/ f+1. \tag{21}$$

The absolute DCS's of the sodium $3P$ excited polarized states were obtained by calibration with respect to the ground-state DCS according to Eq. (21), while the ground-state DCS is normalized to CCC calculated results [26]. DCS of $3P,M_L=+1$ and $3P,M_L=-1$ are listed as well in Table VI as σ^+_{3P} and σ^-_{3P}, respectively. Comparison between present and CCC calculated results is shown in Fig. 9. Generally, the agreement is reasonably good except at 6 and 7 eV where the discrepancies can be as large as a factor of 2.

To the best of our knowledge, the results of the azimuthal asymmetry shown in Fig. 9 are the first observation of the orbital effects in the elastic electron collision due to M_L atomic state perpendicular to the scattering plane. The mag-

nitudes of the measured asymmetry are found to be more pronounced at incident electron energies below 5 eV, approaching zero at higher incident energies. Data show that the asymmetry could be larger than a factor of 0.3 with a confidence level of 90% at the incident electron energies between 1 and 5 eV. The magnitude of this asymmetry, caused by a pure Coulomb interaction, indicates how strong is the dynamical effect caused by the valence electron orbital motion in the atom.

Data presented in this paper examine the relative roles played by the valence electron and the core of the target atom in the collision process. The azimuthal asymmetry, as well as the M_L-dependent DCS measurements, give the next level of detailed, and therefore more stringent test of approximation used for calculation.

ACKNOWLEDGMENTS

This work is supported by the Physics Department of Old Dominion University, and partially by U.S. National Science Foundation, Grant No. PHY-9007571. We thank B. Bederson for valuable discussions, B. L. Whitten and W. K. Trail for sending us results prior to publication, and I. Bray for sending us numerical results of his calculations.

[1] See, for example, *Workshop on Polarized ^{3}He Beams and Targets*, edited by R. W. Dunford and F. P. Calaprice, AIP Conf. Proc. No. 131 (AIP, New York, 1985); A. K. Thompson *et al.*, Phys. Rev. Lett. **68**, 2901 (1992).
[2] N. Anderson, J. W. Gallagher, and I. V. Hertel, Phys. Rep. **165**, 1 (1988).
[3] J. J. McClelland, M. H. Kelley, and R. J. Celotta, Phys. Rev. Lett. **55**, 688 (1985).
[4] J. J. McClelland, M. H. Kelley, and R. J. Celotta, Phys. Rev. Lett. **56**, 362 (1986).
[5] J. J. McClelland, M. H. Kelley, and R. J. Celotta, Phys. Rev. Lett. **58**, 2198 (1987).
[6] S. R. Lorentz, R. E. Scholten, J. J. McClelland, M. H. Kelley, and R. J. Celotta, Phys. Rev. Lett. **67**, 3761 (1991).
[7] J. J. McClelland, S. R. Lorentz, R. E. Scholten, M. H. Kelley, and R. J. Celotta, Phys. Rev. A **46**, 6079 (1992).
[8] V. Nickich, T. Hegemann, M. Bartsch, and G. F. Hanne, Z. Phys. D **16**, 261 (1990).
[9] Z. Shi, C. H. Ying, and L. Vušković, Phys. Rev. A **53**, R16 (1996).
[10] B. Jaduszliwer, P. Weis, A. Tino, and B. Bederson, Phys. Rev. A **30**, 1255 (1984).
[11] L. Vušković, M. Zuo, S. G. Shen, B. Stumpf, and B. Bederson, Phys. Rev. A **40**, 133 (1989).
[12] T. Y. Jiang, C. H. Ying, L. Vušković, and B. Bederson, Phys. Rev. A **42**, 3852 (1990).
[13] Z. Shi, Ph.D. thesis, New York University (1995).
[14] J. J. McClelland, M. H. Kelley, and R. J. Celotta, Phys. Rev. A **40**, 2321 (1989).
[15] T. Y. Jiang, M. Zuo, L. Vušković, and B. Bederson, Phys. Rev. Lett. **68**, 915 (1992).
[16] Z. Shi, C. H. Ying, and L. Vušković (unpublished).
[17] D. A. Dhal and J. E. Delmore, Idaho National Engineering Laboratory, Internal Publication EEG-CS-7233 (1988).
[18] C. E. Kuyatt and J. A. Simpson, Rev. Sci. Instrum. **38**, 103 (1967).
[19] M. Zuo, T. Y. Jiang, L. Vušković, and B. Bederson, Phys. Rev. A **41**, 2489 (1990).
[20] B. Jaduszliwer, R. Dang, P. Weiss, and B. Bederson, Phys. Rev. A **21**, 808 (1980).
[21] B. Jaduszliwer, P. Weiss, A. Tino, and B. Bederson, Phys. Rev. A **30**, 1255 (1984).
[22] B. Jaduszliwer, G. F. Shen, J. L. Cai, and B. Bederson, Phys. Rev. A. **31**, 1157 (1985).
[23] T. Y. Jiang, Ph.D. thesis, New York University (1990).
[24] W. K. Trail, M. A. Morrison, H. L. Zhou, B. L. Whitten, K. Bartschat, K. B. MacAdam, T. L. Goforth, and D. W. Norcross, Phys. Rev. A **49**, 3620 (1994).
[25] B. L. Whitten, W. K. Trail, H. L. Zhou, M. A. Morrison, K. Bartschat, and D. W. Norcross, in Proceedings of the 24th Annual Meeting, Division of Atomic, Molecular and Optical Physics, Cristal City, Virginia, April 1994 [Bull. Am. Phys. Soc. **39**, 1073 (1994)]; B. L. Whitten and W. K. Trail (private communication).
[26] I. Bray, D. V. Fursa, and I. E. McCarthy, Phys. Rev. A **49**, 2667 (1994); I. Bray (private communication).
[27] D. M. Brink and G. R. Satchler, *Angular Momentum* (Oxford University Press, Ely House, London, 1968).